

pubs.acs.org/amrcda Article

# Converting Iron Corrosion Product to Nanostructured Conducting Polymers: Synthetic Strategies and Applications

Yifan Diao,<sup>\$</sup> Haoru Yang,<sup>\$</sup> Yang Lu, Hongmin Wang, Reagan Woon, Alina Chow, Chiemela Izima, Brandon Chow, and Julio M. D'Arcy\*



Cite This: Acc. Mater. Res. 2023, 4, 616-626



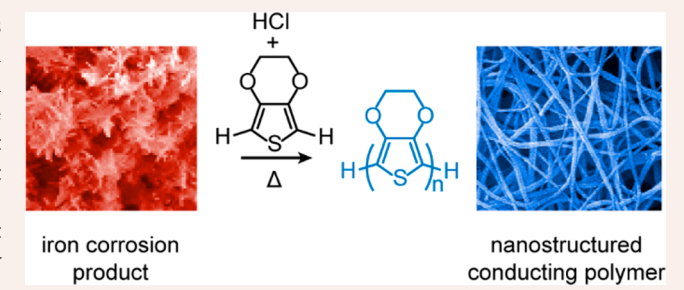
**ACCESS** I

III Metrics & More

Article Recommendations

s Supporting Information

**CONSPECTUS:** Iron corrosion product, commonly known as rust, forms from the chemical reaction between iron and oxygen in the presence of water. It is a heterogeneous solid-state material composed of multiple phases and is ubiquitous throughout the universe. Sixteen distinct phases of iron corrosion product exist naturally under different temperature, pH, and pressure. Rust species such as hematite ( $\alpha$ - Fe<sub>2</sub>O<sub>3</sub>), maghemite ( $\gamma$ -Fe<sub>2</sub>O<sub>3</sub>), goethite ( $\alpha$ -FeOOH), and lepidocrocite ( $\gamma$ - FeOOH), first documented ca. 800 BCE, make up the solid-state chemical family composed of iron oxides, oxyhydroxides, and hydroxides. On an anthropogenic scale, rust represents a persistent problem to all



manner of engineering and industrial pursuits. Corrosion is gradual and nondiscriminatory, affecting iron structures of all shapes and sizes from bridges and buildings to pipelines and wires that necessitates considerable spending on rust prevention and removal techniques. The infamous "Rust Belt" is colloquially used to describe regions of the United States characterized by sharp industrial decline and evokes images of derelict steel factories rusted over from decades of disuse. Therefore, iron corrosion product is commonly regarded as a symptom of deterioration and a physical manifestation of neglect in the eyes of the public. Yet, invaluable scientific potential exists within this "waste" material.

Rust is thermodynamically stable, inexpensive, easily processable, and an abundant source of ferric ions (Fe<sup>3+</sup>) and therefore serves as an attractive oxidative candidate for developing chemical reactions. The ferric ion, with a standard reduction potential of +0.77 V, is an oxidizing agent that is well-investigated in the syntheses of highly conductive conjugated polymers such as poly(3,4-ethylenedioxythiophene) (PEDOT) and polypyrrole (PPy). Additionally, hydrolysis products of ferric ions form various nanostructures and provide diversified growing template for conducting polymers, including rod-shape akageneite ( $\beta$ -FeOOH), fiber-shape goethite ( $\alpha$ -FeOOH), 2D sheet iron oxychloride (FeOCl), and spherical/cubic hematite ( $\alpha$ -Fe<sub>2</sub>O<sub>3</sub>).

In this Account, we introduce our unique synthetic strategies that involve rust and advance the state-of-the-art in chemical synthesis of nanostructured conducting polymers. We utilize products from rust, droplets with rust, and interfaces containing rust to synthesize nanostructured conducting polymer including rust-based vapor-phase polymerization (RVPP), aerosol vapor polymerization (AVP), and condensing vapor-phase polymerization (CVPP). Owing to the high conductivity and high surface area, nanostructured conducting polymers are emerging as hotspots for electrode materials in energy storage devices (i.e., supercapacitors) and solar cells. In the second part of this Account, we discuss how combining our unique synthetic strategies with conventional materials and fabrication techniques produces devices with high figure of merit performance. These devices include a brick supercapacitor as proof-of-concept energy storage masonry material, a 3D microsupercapacitor with a superior and low-cost electrode engineering strategy as well as high energy density larger than a thin-lithium battery, and a dye-sensitized solar cell with an efficiency superior to that of Pt with cost-effective fabrication.

#### 1. INTRODUCTION

Iron corrosion is one of the most widely recognized oxidative processes in nature, and its heterogeneous corrosion product, rust, is ubiquitous throughout the universe. Rust is commonly understood as the reddish-brown coating of ferric oxide/oxyhydroxide/hydroxide that envelops and corrodes iron surfaces as they react with oxygen in the presence of water. Hematite  $(\alpha\text{-Fe}_2\text{O}_3)$  (Figure 1), an iron oxide polymorph, is the rusty mineral that gives Mars its distinctive red hue and

was recently found widespread at the Moon's lunar poles.<sup>1</sup> Here on Earth, rust can be found thriving in even the most

Received: March 28, 2023 Revised: June 6, 2023 Published: June 21, 2023





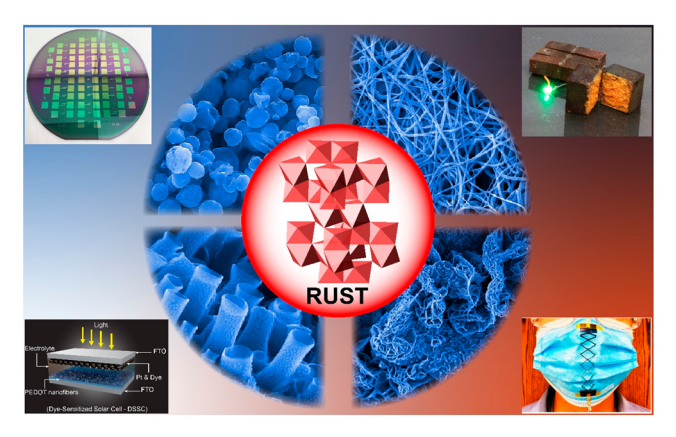


**Figure 1.** Schematic diagram of iron corrosion product (rust) as both a source of Fe<sup>3+</sup> for vapor-phase synthesis of conducting polymers and templates for nanostructure formation. The nanostructured conducting polymers are utilized in energy storage devices, dye-sensitized solar cells, and sensors. Reproduced with permission from ref 38. Copyright 2020 Springer Nature. Reproduced with permission from ref 55. Copyright 2019 Royal Society of Chemistry.

unlikely climates. In the polar desert of Antarctica, five stories of rusty red saltwater pour out from Taylor Glacier in a striking sight known as "Blood Falls" which contains ferric ion-rich saltwater.<sup>2</sup> Although corrosion is a natural phenomenon that produces remarkable natural wonders, humankind has long regarded rust as an unwanted pestilence. Therefore, rust is commonly regarded as a symptom of deterioration and a physical manifestation of neglect in the eyes of the public. Yet, ample value exists even within this "waste" material.

Currently, the value of rust originates from the fact that it is a stable, low cost, and environmentally benign precursor, such as hematite nanoparticles (Fe<sub>2</sub>O<sub>3</sub> NPs), that bear catalytic property<sup>3</sup> and multistate redox activity.<sup>4</sup> Rust-derived Fe<sub>2</sub>O<sub>3</sub> NPs have been successfully applied as catalysts for organic synthesis,<sup>5</sup> photocatalysts for dye degradation,<sup>6</sup> hydrogen evolution,<sup>2</sup> and redox-active electrodes for batteries.<sup>4</sup> Here, we provide another angle where the potential of rust and the rusting process are harnessed, i.e. redox potential of Fe<sup>3+</sup> that activates radical polymerization of conducting polymers and the rusting process that guides the growth of a nanostructured conjugated polymer film.<sup>7</sup>

Conjugated polymers, such as poly(3,4-ethylenedioxythiophene) (PEDOT) and polypyrrole (PPy), are a class of organic semiconducting materials that possess both electrical and ionic conductivity.8 Most conjugated polymers are synthesized using oxidative radical polymerization which is initiated by oxidizing monomers into reactive radicals. Polymer chains subsequently grow via coupling between monomer radicals, followed by removing excess protons. Oxidants and proton scavengers thus play a pivotal role throughout the reaction. 10 Commonly used aqueous Fe<sup>3+</sup> solution in a polymerization reaction often involves complications such as liquid surface tension, pH, and the hydrolysis of Fe<sup>3+</sup>.<sup>11</sup> These constraints are mitigated with powdery and mechanically robust solid-phase rust. Rust is thermodynamically stable and naturally occurring source of Fe<sup>3+</sup>, which makes it an ideal oxidant precursor for conjugated polymer synthesis. 12 Fe<sup>3+</sup> ion hydrolysis products also provide diversified growing templates due to the rich structural chemistry of the rusting process, 13 such as rod-shape akageneite ( $\beta$ -FeOOH), fiber-shape goethite ( $\alpha$ -FeOOH)/ lepidocrocite ( $\gamma$ -FeOOH), and spherical and cubic hematite

(α-Fe<sub>2</sub>O<sub>3</sub>). Researchers have reported using size-controlled iron rust nanoparticles for templated conducting polymer composite synthesis in the past decade. Akageneite (β-FeOOH) contains chloride-filled channels in its crystal structure, which makes it an ideal component in a nanocomposite with polyaniline for chromium ion removal. Other phases such as lepidocrocite (γ-FeOOH) consists of two-dimensional layered structure, and its interlayer distance is useful for ion transport. A composite between polypyrrole and lepidocrocite results in a supercapacitor electrode with high capacitance and cycle stability.

In our strategy, oxidative radical polymerization changes the course of hydrolysis, captures nanostructured hydrolysis intermediates to serve as the template, and further promotes templated growth. The interplay between iron hydrolysis and oxidative radical polymerization leads to highly conductive conjugated polymers with varied nanostructures. In this Account, we summarize recent progress in rust chemistry and new strategies on synthesizing nanostructured conducting polymers by investigating oxidative radical polymerization. We introduce various synthetic approaches that take advantage of iron corrosion as well as its product to generate distinct nanostructured conducting polymers and demonstrate our contribution to diverse applications in energy storage and solar cells. Additional discussions on related synthetic techniques and applications such as humidity sensing are in the Supporting Information.

### 2. SYNTHESIS OF CONDUCTING POLYMER NANOSTRUCTURES

Nanostructured conducting polymers are superior to conventional bulk-phase conducting polymers and show improved electrical conductivity, carrier mobility, electrochemical activity, optical property, and biocompatibility thanks to the well-defined nanostructure and high surface area. <sup>17</sup> Depending on applications, conducting polymers are synthesized as 0D nanospheres, 1D nanofibers/rods/wires/tubes, 2D nanosheets, 3D porous structures, and nanohybrids with monolithic or core—shell structures. However, structural defects, inhomogeneous aggregation, severe restacking, and poor contact destroy the advanced properties of nanostructured conducting polymers; therefore, controlling the morphology is of paramount importance. <sup>17</sup>

Among various synthetic strategies, vapor-phase polymerization produces a contiguous crystalline film with minimal boundary and showing the highest conductivity. Here, we explore template-free vapor-phase polymerizations for synthesizing conducting polymer nanostructured films/coatings. We introduce strategies that utilize rust and droplets with rust to synthesize nanostructured conducting polymers, including rust-based vapor-phase polymerization (RVPP), aerosol vapor polymerization (AVP), and condensing vapor-phase polymerization (CVPP).

#### 2.1. Rust-Based Vapor-Phase Polymerization (RVPP)

Currently, polymerization from the vapor phase usually requires a metal salts serving as the oxidizing agent, such as Fe<sup>3+</sup>-containing salts.<sup>21</sup> However, such an approach suffers from the following: (1) Costly fabrication, since Fe<sup>3+</sup>-containing salts are expensive and its corrosive properties require safety precautions during handling.<sup>22</sup> (2) Poor reproducibility, since Fe<sup>3+</sup> salts are hygroscopic, chemically unstable, and undergo hydrolysis over time.<sup>11,13</sup> (3) Limited

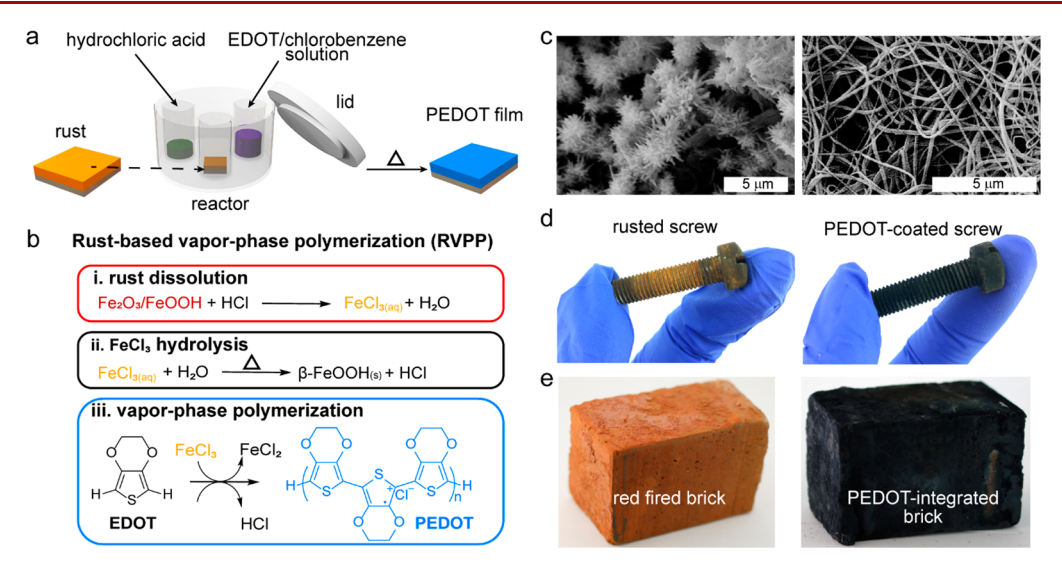


**Figure 2.** (a) Schematic diagram of rust-based vapor-phase polymerization (RVPP) carried out in a sealed vessel. (b) Scheme of RVPP mechanism entailing rust dissolution, Fe<sup>3+</sup> hydrolysis, and oxidative radical polymerization of EDOT monomer into a doped form of PEDOT. (c) Scanning electron micrograph shows that rust possesses sea-urchin-like microstructure and is converted to a nanofibrillar architecture with high packing density of high aspect ratio nanofibers. (d and e) Photographs show that a rusted screw and red fired brick serve as substrates for RVPP, leading to conformal blue texturized PEDOT coatings. Reproduced with permission from ref 7. Copyright 2019 American Chemical Society.

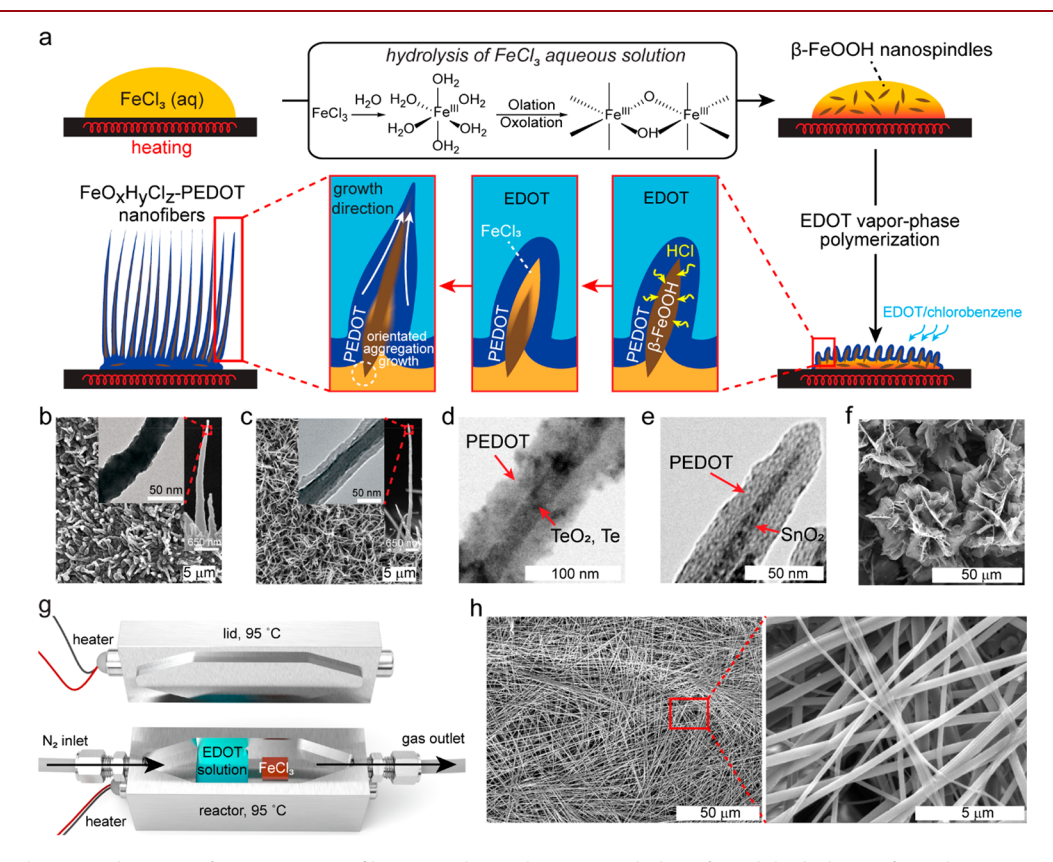


Figure 3. (a) Schematic diagram of PEDOT nanofiber growth mechanism, including forced hydrolysis of FeCl<sub>3</sub> in water into β-FeOOH nanospindles that templates the oxidative radical vapor-phase polymerization of EDOT into PEDOT nanofibers. The polymerization produces Cl<sup>-</sup>doped PEDOT and byproduct HCl that etches the β-FeOOH core and liberates more FeCl<sub>3</sub> for reaction. Control of pH enables the synthesis of (b) monolithic PEDOT nanofibers and (c) FeO<sub>x</sub>H<sub>y</sub>Cl<sub>z</sub>-PEDOT core—shell nanofibers. Hydrolysis of TeCl<sub>4</sub> and SnCl<sub>4</sub> lead to (d) TeO<sub>x</sub>-PEDOT core—shell nanostructure and (e) SnO<sub>2</sub>-PEDOT core—shell nanorods. (f) Hydrolysis of FeCl<sub>3</sub> in organic solvent (ethanol) produces FeOCl 2D nanostructure that templates 2D PEDOT nanoflower synthesis. (g) Modification of the reactor adding a N<sub>2</sub> bypass increases mass transport efficiency of EDOT vapor and enables the synthesis at temperatures lower than 130 °C. (h) Horizontally directed PEDOT nanofibers are synthesized with nucleation control and self-assemble into a 3D network mat. Reproduced with permission from ref 10. Copyright 2018 American Chemical Society. Reproduced with permission from ref 33. Copyright 2019 Royal Society of Chemistry.

versatility, since Fe<sup>3+</sup>-containing solution and vapor are affected by template hydrophilicity/hydrophobicity (droplet morphology) and container materials (glass or stainless steel) leading to nonuniform and unrepeatable polymer morphology.<sup>23</sup> We present a robust solid-state platform for synthesizing nanostructured conducting polymer utilizing rust as a reactant, named rust-based vapor-phase polymerization (RVPP).<sup>7</sup> This approach obviates the need of a corrosive salt, affords a stable solid-state oxidant source for engineering facile reactions, and provides a sustainable approach for the synthesis of organic electronics using what is typically considered chemical waste.

Rust-based vapor-phase polymerization (RVPP) advances the state-of-the-art in chemical synthesis via deposition of freestanding nanofibrillar films of the conducting polymer poly(3,4-ethylenedioxythiophene) (PEDOT) on a rust-containing substrate. A nanofibrillar PEDOT film is synthesized by placing a rusted steel sheet in a sealed vessel along with 20  $\mu$ L of concentrated hydrochloric acid and 200  $\mu$ L of a 0.0034 M EDOT in chlorobenzene solution (Figure 2a). As the temperature initially ramps up, hydrochloric acid vapor diffuses, dissolves rust, and liberates Fe<sup>3+</sup> ions. Fe<sup>3+</sup> ions simultaneously undergo hydrolysis and oxidize monomer molecules upon contact (Figure 2b). During oxidative radical polymerization, some Fe<sup>3+</sup> ions oxidize monomer 3,4-ethylenedioxythiophene (EDOT) molecules to EDOT+• radical cations. These radicals couple together and form the conjugated PEDOT backbone via step-growth polymerization.<sup>24</sup> Throughout this process, monomer-radical coupling and deprotonation occur repeatedly. Other Fe<sup>3+</sup> ions undergo hydrolysis due to elevated temperature, forming sea-urchin-like structures (Figure 2c, left), and templates the growth of PEDOT into a nanofibrillar morphology (Figure 2c, right) doped by chloride ions.

Due to this solid-phase conversion, chemistry enabled by rust provides an opportunity for integrating conducting polymer with any rust containing materials. As a proof of concept, a corroded metal screw (Figure 2d) and a brick (Figure 2e) are successfully converted to a PEDOT-coated screw and PEDOT-integrated brick.

### 2.2. Hydrolysis-Assisted Vapor-Phase Polymerization (HVPP)

Core—shell system is promising due to its hybrid functionality in both core and shell that shows a synergistic effect in energy storage, <sup>25</sup> photothermal therapy, <sup>26</sup> electromagnetic absorption <sup>27</sup> and photoluminescence. <sup>28</sup> Current synthetic strategies, including hard-templating, soft-templating, and template-free, suffer from restricted scale, high-cost, and difficulty in template elimination. <sup>18</sup> To overcome those limitations, we developed hydrolysis-assisted vapor-phase polymerization (HVPP) by utilizing a FeCl<sub>3</sub> droplet. <sup>10</sup>

Fe<sup>3+</sup> dissolved in water undergoes hydrolysis, producing hexa-aqua complexes  $[Fe(H_2O)_6]^{3+}$  which readily undergo substitution reactions (olation and oxolation) and form Fe—OH–Fe and Fe–O–Fe polymers (Figure 3a). Hydrolysis-assisted vapor-phase polymerization (HVPP) "hijacks" the formation of inorganic polymers during hydrolysis to template conducting polymer synthesis. A Cl<sup>-</sup>-rich environment and low pH contribute to the precipitation of  $\beta$ -FeOOH nanospindles at elevated temperature (130 °C). During synthesis,  $\beta$ -FeOOH nanospindles serve as preferential nucleation sites, resulting in 1D conducting polymer nanofibers of a high aspect-ratio (~500). The pH offers control over the structure of 1D

conducting polymer nanofibers because iron species are etched at a faster rate under low pH. This leads to formation of monolithic PEDOT nanofibers (Figure 3b), while higher pH leads to FeO<sub>x</sub>H<sub>y</sub>Cl<sub>z</sub>–PEDOT core—shell nanofibers (Figure 3c).<sup>29</sup> Core—shell nanofibers are further controlled by utilizing a two-salt system with FeCl<sub>3</sub> as the oxidant for polymerization while more hydrolysis-prone salts such as TeCl<sub>4</sub> and SnCl<sub>4</sub> are introduced to serve as templates.<sup>30</sup> This system promotes forced hydrolysis of TeCl<sub>4</sub> and SnCl<sub>4</sub> to produce TeO<sub>2</sub> nanowires (Figure 3d) and SnO<sub>2</sub> nanorods (Figure 3e) that serve as cores in inorganic oxide–PEDOT core—shell hybrid nanomaterials.<sup>31</sup> Alternatively, nanostructure is controlled by the polarity of the solvent. For example, hydrated solvents such as ethanol and nitromethane produce 2D FeOCl templates that result in 2D PEDOT nanoflowers (Figure 3f).<sup>32</sup>

Altering the stoichiometry and temperature affects initial nucleation of  $\beta$ -FeOOH and determines the growth direction of PEDOT nanofibers. Under high FeCl<sub>3</sub> concentration (saturated) and low temperature (95 °C), hydrolysis is stifled and  $\beta$ -FeOOH nanospindles nucleate in a slow and heterogeneous manner on the substrate. Horizontally directed nanofibers develop along the substrate, minimizing the overall system energy and eventually self-assembling into a porous mat. Mass transport of EDOT vapor is enhanced with N<sub>2</sub> gas flow because the low temperature diminishes evaporation of the monomer solution (Figure 3g). Horizontally directed PEDOT nanofibers possess a high aspect-ratio of  $\sim$ 1000 with high packing density and form a 23  $\mu$ m thick 3D network (Figure 3h).<sup>33</sup>

### 3. STRUCTURE DESIGN AND ENGINEERING IN CONDUCTING POLYMER-BASED DEVICES

#### 3.1. Energy Storage: Supercapacitors

A supercapacitor or electrochemical capacitor is an energy storage device consisting of two electrically conductive electrodes separated by an electrolyte with mobile ions. This device features fast charging—discharging rates and long-term cycle stability because nanostructured electrodes provide large surface area that stores energy in both electric double layers and redox-active sites; additionally, high free volume mitigates mechanical deformation and facilitates ion transport. The supercharge of two electrochemical deformation and facilitates in transport.

## **3.1.1. Stationary Supercapacitor Based on Red Brick.** Finding a solution for large-scale energy storage is of paramount importance in accordance with the development

paramount importance in accordance with the development of renewable energy. Molten electrodes used for commercialized large-scale energy storage, such as the sodium—sulfur battery, feature low cost, high energy density, long cycle life, and high Coulombic efficiency.<sup>36</sup> However, the high operating temperature (≥300 °C) raises maintenance cost, safety issues, and battery corrosion; development of a room temperature sodium—sulfur battery is in its infancy.<sup>37</sup> Other electrochemical energy storage technologies such as lithium ion batteries are unsuitable for large scale applications due to the high price and low lithium abundance. We propose a concept of storing energy in building walls by creating an electrochemically active coating on construction materials.<sup>38</sup>

Fired red brick is a 5000-year-old construction material containing fused particles of  $SiO_2$ ,  $Al_2O_3$ , and  $\alpha$ -Fe<sub>2</sub>O<sub>3</sub>. <sup>39</sup> Polymer nanofibers are deposited within the inorganic matrix of a brick to develop supercapacitors. This process is initiated by the liberation of Fe<sup>3+</sup> from the hematite in a brick. The

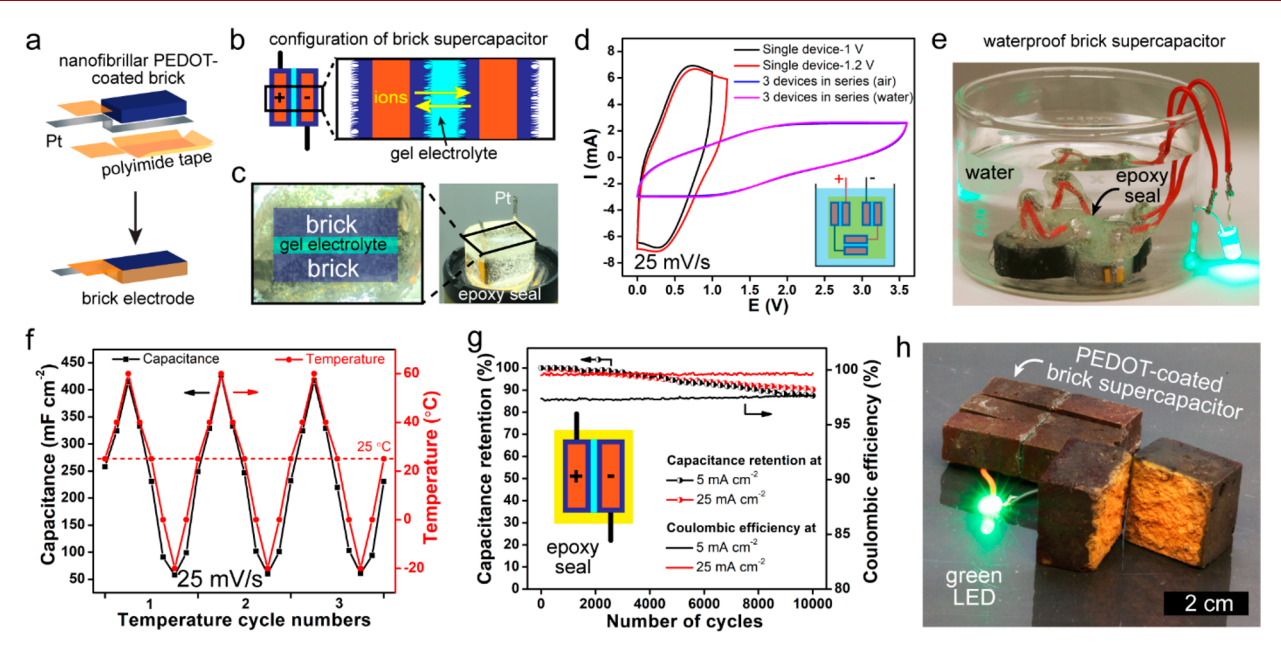


Figure 4. Red fired brick-based PEDOT supercapacitor. (a) Working electrode configuration containing a nanofibrillar PEDOT-coated brick and a Pt current lead. (b, c) Two-electrode supercapacitor configuration utilizing gel electrolyte sealed in epoxy. (d) Cyclic voltammograms of a single gel electrolyte supercapacitor with extended voltage window up to 1.2 V and a tandem device containing three supercapacitors showing a 3.6 V voltage window. Epoxy seal contributes to a waterproof device exhibiting identical cyclic voltammograms before/after being submerged under water. (e) The waterproof device lights up a green LED when submerged under water. (f) The gel electrolyte supercapacitor stores charge at temperatures between -20 and 60 °C and (g) remains stable after 10 000 charge—discharge cycles in ambient conditions. (h) A modularized tandem brick supercapacitor lights up a green LED. Reproduced with permission from ref 38. Copyright 2020 Springer Nature.

brick's microporous structure enables facile diffusion of reagent vapors that contributes to robust adhesion with PEDOT. A PEDOT-coated brick is converted to a working electrode for carrying out cyclic voltammetry (three-electrode geometry) by attaching a Pt current lead with polyimide tape (Figure 4a). Two-electrode supercapacitors are fabricated using gel (poly-(vinyl alcohol) + 1 M H<sub>2</sub>SO<sub>4</sub>) electrolytes. while application of gel electrolyte to one brick face allows charge storage on the opposite face (Figure 4b). Gel electrolyte is utilized to enhance device stability and minimize electrolyte leakage, acting as both a binder and separator to mimic a "brick-mortar-brick" structure. Gel electrolyte is selected because of its excellent processability and ionic conductivity, and epoxy is utilized as a sealant (Figure 4c), producing a stable waterproof supercapacitor. The supercapacitor exhibits an areal capacitance of  $0.868 \text{ F/cm}^2$  and areal energy density of  $121 \mu \text{Wh/cm}^2$ . Connecting three devices creates a waterproof system as evidenced by identical cyclic voltammograms before and after being submerged (Figure 4d) and extends the voltage window to 3.6 V, lighting up a green LED (Figure 4e). The brick supercapacitor is operational between -20 and 60 °C and remains stable after three heating-cooling cycles (Figure 4f). Gel electrolyte and epoxy sealing enable 10 000 chargedischarge cycles with  $\sim 90\%$  capacitance retention (Figure 4g). The device is easily scaled up and modularized for powering microdevices embedded in the wall (Figure 4h).

**3.1.2.** Three-Dimensional Nanofibrillar Microsupercapacitor. Microsupercapacitors ( $\mu$ SCs) are an attractive alternative to batteries for electrochemical energy storage in miniaturized portable electronics due to their high-power density and extended cycling stability. The challenge for this device is poor energy density, and an efficient approach is to generate 3D structures in an electrode that offer high surface area for charge storage. <sup>40</sup> Current fabrication strategies, such as

inkjet printing,<sup>41</sup> laser scribing,<sup>42</sup> or electrochemistry,<sup>43</sup> require prefabricated templates that unfortunately possess low packing density and low aspect ratio scaffolds with low surface area.<sup>44</sup> We introduce an electrode engineering platform to produce 3D nanofibrillar PEDOT  $\mu$ SCs by combining conventional microfabrication and rust-based vapor-phase polymerization (Figure 5a).<sup>45</sup> Microfabrication of an interdigitated electrode requires spin coating photoresist on SiO<sub>2</sub> and photolithography to produce an interdigitated pattern via laser writer. A chromium adhesion layer, gold current collector, and iron oxide (Fe<sub>2</sub>O<sub>3</sub>) oxidant precursor are sequentially deposited, forming an Fe<sub>2</sub>O<sub>3</sub>-coated electrode. PEDOT nanofibers are deposited (via RVPP) and remain intact after lift-off as interdigitated electrodes that adhere to the current collector (Figure 5b).

A  $\mu$ SC is composed of two five-finger electrodes homogeneously coated with PEDOT nanofibers; each finger and interdigitated gap are 200  $\mu$ m wide (Figure 5c). A high packing density of vertically aligned nanofibers (Figure 5d) is produced due to polymerization in confined volume within the photoresist trenches. A single nanofiber possesses an aspect ratio ~100 (10  $\mu$ m length, 100 nm diameter) (Figure 5e) and core—shell structure (Figure 5f). Energy-dispersive X-ray spectroscopy elemental maps show a homogeneous distribution signal of sulfur, confirming the uniformity of PEDOT nanofibers (Figure 5g).

The interdigitated (L0) and fractal (L1) electrodes are compared to evaluate the electrochemical performance of the  $\mu$ SC configuration (Figure 5h). These devices possess a 200  $\mu$ m gap and are characterized by equivalent series resistance (ESR) of ~13  $\Omega$  and ~17  $\Omega$ , respectively. Unlike 2D electrodes, where ESR increases with complexity in electrode geometry, L1 possesses lower ESR than L0 and a 10% capacitance increase because its vertically directed nanofibrillar

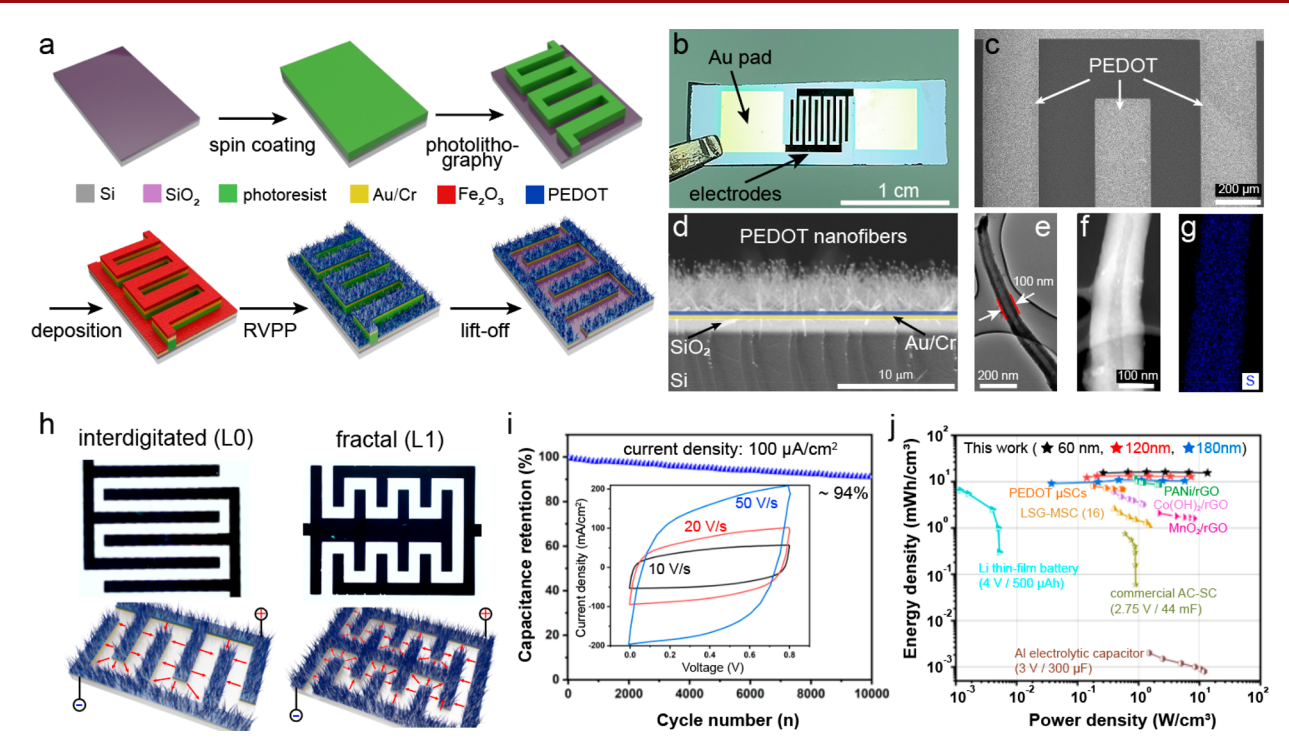
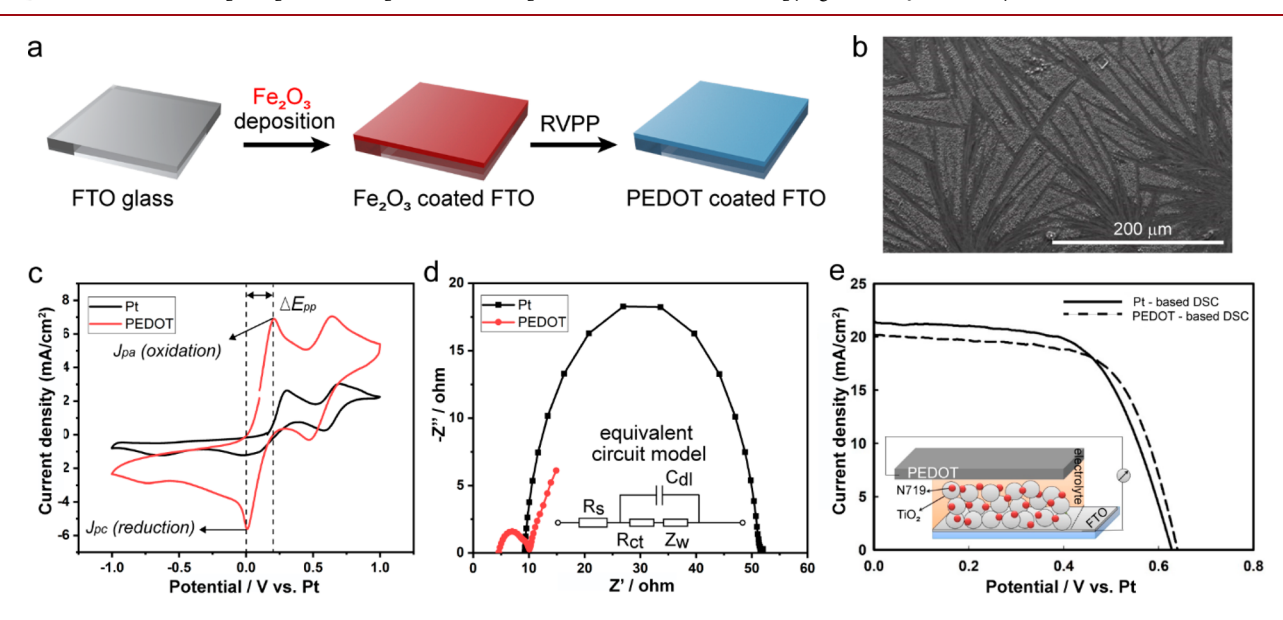


Figure 5. (a) Fabrication process and structural characterization of a 3D nanofibrillar PEDOT  $\mu$ SC. (b) Digital photograph shows the  $\mu$ SC configuration consisting of two electrodes with gold pads and each possessing five PEDOT-coated fingers. (c) A scanning electron micrograph shows a close-up of 200  $\mu$ m wide polymer-coated fingers and demonstrates a gap void of the polymer. (d) Cross-sectional electron micrograph captures device layers (augmented by color) and the active polymer coating composed of a carpet of vertically directed PEDOT nanofibers. (e) Transmission electron micrograph and (f) high-angle annular dark-field STEM image of single fibers confirm a core—shell structure. (g) EDX maps for a nanofiber show an elemental composition consisting of S. (h) Schematic representations of interdigitated (L0) and fractal electrodes (L1) possessing a 200  $\mu$ m gap. (i) After 10 000 cycles with a gel electrolyte, 94% of original capacitance is retained and rectangular-shaped cyclic voltammograms are obtained at scan rates of 10, 20, and 50 V/s. (j) Volumetrically normalized Ragone plot compares our  $\mu$ SCs with a 2D lithium film battery, Al electrolytic capacitor, and activated carbon commercial supercapacitor as well as 2D PEDOT-, PANi/rGO-, Co(OH) $_3$ /rGO-, and MnO $_2$ /rGO-based microsupercapacitors. Reproduced with permission from ref 45. Copyright 2020 John Wiley and Sons.



**Figure 6.** (a) Schematic diagram of PEDOT-based dye-sensitized solar cell fabrication. (b) Scanning electron micrograph of PEDOT film on FTO substrate. (c) Cyclic voltammograms of Pt and PEDOT film as counter electrodes for DSSC at a scan rate of 50 mV/s. (d) Nyquist plots of the symmetric CE-CE cells and the equivalent circuit models for the I $^-$ /I $_3$  $^-$  reaction. (e) Photocurrent-voltage characteristics of DSSCs with PEDOT and Pt CEs under AM 1.5 and schematic of a DSSC using a PEDOT film as a CE (inset). Reproduced with permission from ref 49. Copyright 2020 Elsevier.

structure provides accessible ion pathways. These results highlight the synergistic convergence between fractal geometry

and 3D nanofibrillar electrode architecture, demonstrating low impedance, high capacitance, and a cost-effective fabrication

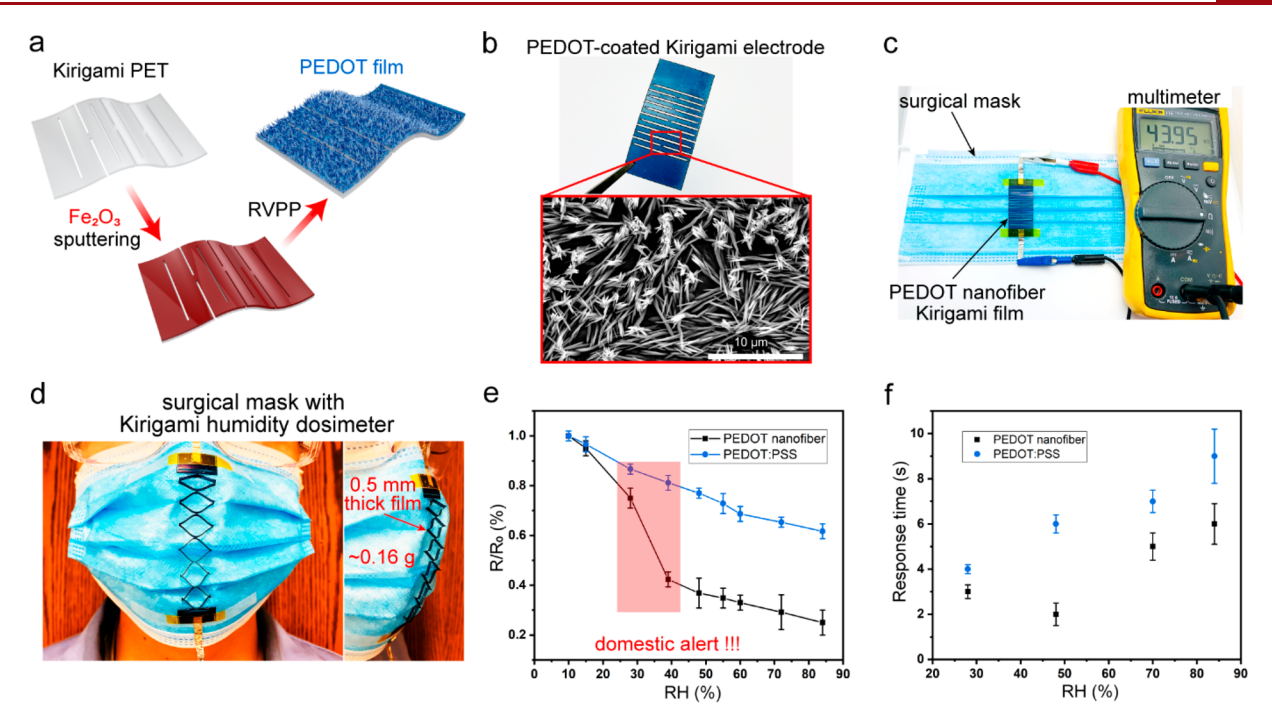


Figure 7. Nanofibrillar PEDOT coatings for a kirigami humidity dosimeter. (a) A kirigami PET film is sputtered with a 60 nm  $Fe_2O_3$  layer and subsequently undergoes rust-based vapor-phase polymerization that produces (b) homogeneous PEDOT nanofibrillar electrode. (c) Photograph of humidity dosimeter in its 2D state attached to a surgical mask. (d) Front and side view of our device stretching to accommodate 3D deformation from surgical mask. (e) Resistance changes and (f) response times compared between PEDOT nanofibers and PEDOT:PSS as a function of relative humidity. Reproduced with permission from ref 55. Copyright 2019 Royal Society of Chemistry.

strategy. A 1 M  $\rm H_2SO_4/poly(vinyl\ alcohol)$  (PVA) gel electrolyte is applied to minimize electrolyte leakage and enhance cycling stability, allowing a  $\mu$ SC to retain 94% original capacitance after 10 000 cycles whereas liquid water-based devices retain 90%. The gel  $\mu$ SCs exhibit symmetric rectangular CVs (50 V/s scan rate) due to a highly ordered nanofibrillar surface area as well as low electronic and ionic resistances (Figure 5i). A Ragone plot compares power density to energy density and evaluates energy storage metrics after normalizing figures of merit by volume or area (Figure 5j). A device with a 250 nm polymer coating exhibits a volumetric energy density of 16.1 mWh/cm³ while a coating thickness of 900 nm achieves an areal energy density of 1.9 mWh/cm². These values represent the highest performance for conducting polymer-based  $\mu$ SCs, surpassing Li-thin film battery metrics.

#### 3.2. Dye-Sensitized Solar Cells

Dye-sensitized solar cells (DSSCs) are an attractive alternative to traditional photovoltaic devices due to their low cost, simple manufacturing process, and high theoretical photoelectric conversion efficiency. 46 DSSCs typically consist of a TiO<sub>2</sub> electrode sensitized with an absorbing layer, an electrolyte, and a Pt counter electrode (CE). The CE acts as the reducing agent in a redox couple, collects electrons from the external circuit, transmits them back into the cell, and reflects unabsorbed light back into the cell to enhance utilization of sunlight energy.<sup>47</sup> An ideal CE possesses high catalytic activity, high conductivity, high reflectivity, high surface area, high electrochemical and mechanical stability, low cost, and good adhesion to the substrate. We fabricate a cost-effective DSSC with a PEDOT  $CE^{49}$  by sputtering a 40 nm thick  $Fe_2O_3$ oxidant layer on a piece of fluorine-doped tin oxide (FTO) and then converting the Fe<sub>2</sub>O<sub>3</sub> layer to polymer via chemical synthesis (Figure 6a). A high surface area PEDOT nanofibrillar

film is deposited via RVPP<sup>7</sup> onto the FTO glass substrate and is characterized by a conductivity of 1021 S/cm (Figure 6b).

To evaluate the electrochemical performance of a PEDOT vs Pt CE, cyclic voltammetry is carried out to probe the charge transfer process and electrocatalytic activity in iodine redox electrolyte with a three-electrode system. The anodic  $(I_{pa})$  and cathodic  $(I_{pc})$  peak correspond to the oxidation of I<sup>-</sup> and the reduction of I<sub>3</sub><sup>-</sup>, respectively (Figure 6c). There is a significant increase in the  $J_{\rm nc}$  for PEDOT (6.0 mA/cm<sup>2</sup>) compared to the Pt electrode (2.7 mA/cm<sup>2</sup>), indicating excellent electrocatalytic ability of the PEDOT film to reduce  $I_3^{-50}$  Moreover, the lower peak potential separation ( $\Delta E_{pp}$  = potential difference between the  $J_{pa}$  and  $J_{pc}$ ) for PEDOT indicates a faster reaction rate for the reduction of I<sub>3</sub><sup>-</sup> to I<sup>-</sup>. These results suggest that a PEDOT CE is a highly efficient electrochemical catalyst due to fast electron transport at the electrode/electrolyte interface, resulting in an increased rate of reduction of I<sub>3</sub><sup>-</sup> to I<sup>-</sup>. Nyquist plot is introduced to evaluate the impedance of Pt and PEDOT cells (Figure 6d), and the equivalent RC circuit model (Figure 6d inset) is used to obtain the EIS parameters  $(R_S, R_{ct}, Z_w)$  by fitting the impedance spectra to the equivalent model. The  $R_s$ value refers to the equivalent series resistances (ESR: x-axis intercept) and is associated with the contact resistance between current collector and CE, the resistance of CE, and the resistance of electrolyte and CE interface. Our PEDOT CE possess a lower ESR (4.3  $\Omega$ ) compared to Pt (9.2  $\Omega$ ). The diameter of the semicircle represents both the charge transfer resistance  $(R_{ct})$  at the CE/electrolyte interface and the redox species  $(I^-/I_3^-)$  diffusion resistance  $(Z_w)$  in the electrolyte. The  $R_{\rm ct}$  for the PEDOT film (7  $\Omega$ ) is six times lower than that for the Pt film (42  $\Omega$ ), suggesting a higher charge transfer process at the electrolyte/PEDOT CE interface due to the

high conductivity and catalytic activity of the PEDOT that facilitates electron transfer. 51

A DSSC full cell is fabricated utilizing FTO/TiO<sub>2</sub> as the working electrode and PEDOT as the CE (Figure 6e inset), and the photovoltaic performance is evaluated under ambient conditions. The photocurrent density—photovoltage (J–V) (Figure 6e) shows similar open-circuit voltage for both cells; the PEDOT—DSSC possesses a high short-current density (20.24 mA/cm²) which is slightly lower than Pt—DSSC due to PEDOT's higher intrinsic electrical conductivity. However, a higher fill factor (FF) (65%) value is observed for PEDOT film due to its low  $R_{\rm ct}$  and excellent electrochemical catalytic activity, attributed to the increased contact area between the PEDOT CE and electrolyte. <sup>52</sup> As a result, the PEDOT—DSSC exhibits 8.4% higher efficiency compared to the values reported in the literature.

#### 3.3. Kirigami Humidity Dosimeter

Wearable healthcare monitors are emerging as hotspots in scientific research due to their extended applications in medical science and smart electronics. Kirigami, the art of paper cutting, is an emerging approach to constructing stretchable 3D architectures out of simply cutting planar sheets. Under external strain, cuts made in thin films undergo in-plane rotation and out-of-plane buckling that expand to 3D structures. However, these thin film electrodes suffer from limited surface area and are characterized by poor sensitivity. The field of kirigami is consequently experiencing a lack of applications in healthcare-sensing devices. We demonstrate refined control over deposition of conducting polymer nanofibers on kirigami film for humidity dosimeters via our previously reported rust-assisted vapor-phase polymerization (RVPP).

A conformal PEDOT nanofibrillar film is produced by sputtering an oxidant precursor (Fe<sub>2</sub>O<sub>3</sub>) onto a kirigami polyethylene terephthalate (PET) film (Figure 7a) via previously reported synthesis (RVPP). Scanning electron micrographs (SEM) in Figure 7b show homogeneous PEDOT (blue) thin films with nanofibers growing up to an aspect ratio of 50, generating a high surface area, high packing density, and conducting network. Due to the global outbreak of COVID-19, the ability to detect whether one's mask has been exposed to respiratory droplets from coughing or sneezing is also of considerable importance.<sup>56</sup> Our nanofibrillar PEDOT kirigami electrode serves as a flexible chemoresistive sensor by monitoring the relative humidity change on the mask to detect droplet attachment.<sup>57</sup> The stretchable 2D kirigami electrode is easily integrated onto the 2D mask via platinum current leads, Kapton tape, and a multimeter (Figure 7c), and it shows clear compatibility mechanically with a surgical mask at a thickness of only 0.5 mm and a mass of 0.16 g.

For comparison, we introduce our nanofibrillar PEDOT electrode and compared it against PEDOT:PSS thin film electrodes for testing humidity levels. Figure 7d shows that the resistance decreases with increasing humidity for both electrodes due to (1) polymer swelling-induced electron transfer through conjugation length, and (2) formation of a water layer that induces electron hopping and facilitates electron transfer. Importantly, the nanofibrillar PEDOT film exhibits remarkable decrease in resistance at the initial humidity range (around 40% relative humidity) and exhibits faster response (<2 s) in comparison to the PEDOT:PSS thin film (Figure 7e). The heightened response of our electrode is

a consequence of the larger surface area generated by high aspect ratio nanofibers that provide more accessible pathways for water vapor to traverse. <sup>59</sup> This is congruent with the porous nature of nanofiber films, in which gas molecules or aerosol droplets can rapidly diffuse in and out of the nanofibers (Figure 7f). <sup>60</sup> Our PEDOT nanofibrillar humidity dosimeter exhibits better performance in both sensitivity and response time than conventional PEDOT:PSS films as well as commercial humidity sensors, qualifying it as an ideal humidity-sensing dosimeter accessory for surgical masks.

#### 4. CONCLUSIONS AND OUTLOOK

Iron corrosion products are useful materials owing to their interesting properties. They are both ideal solid-state sources of Fe<sup>3+</sup> ions for carrying out chemical synthesis and templates for nanostructured conducting polymer synthesis. Our technique provides a simpler approach to synthesizing highly conductive PEDOT and polypyrrole nanostructures ranging from nanofibrillar and nanotubular film to submicron particles. Vapor-phase synthetic techniques such as HVPP and RVPP produces homogeneous nanostructured PEDOT films. The polymer film is composed of 1D nanofibers with high packing density and possesses enhanced electrical conductivity. Our vapor-phase deposition technique is applicable to both inorganic (silicon, conductive FTO glass, fired brick) and organic (PET) substrates. We demonstrated the versatility of vapor-phase-synthesized conducting polymer films with a variety of applications such as energy storage, solar cells, and sensing. Future research will include overcoming challenges in mass transport of reactants to facilitate scaling up of our vaporphase techniques. Potential solutions include utilizing active transport methods, such as flowing vapors with a carrier gas. We envision that the enriched product forms of nanostructured conducting polymer will enhance performance in fields of energy storage, electro/photocatalysis, sensing, electromagnetic interference shielding, and mixed ionicelectronic electronics.

#### ASSOCIATED CONTENT

#### Supporting Information

The Supporting Information is available free of charge at https://pubs.acs.org/doi/10.1021/accountsmr.3c00031.

Summary of electrical conductivities; other vapor-phase synthetic strategies of nanostructured conducting polymers (PDF)

#### AUTHOR INFORMATION

#### **Corresponding Author**

Julio M. D'Arcy — Institute of Materials Science & Engineering and Department of Chemistry, Washington University, St. Louis, Missouri 63130, United States; Present Address: Department of Chemistry and Biochemistry, Clark University, Worcester, MA 01610.; oorcid.org/0000-0002-6823-3586; Email: judarcy@clarku.edu

#### **Authors**

Yifan Diao – Institute of Materials Science & Engineering, Washington University, St. Louis, Missouri 63130, United States; Present Address: Central R&D Institute, LONGi Green Energy Technology Co. Ltd., Shanghai 200120, China Haoru Yang — Department of Chemistry, Washington University, St. Louis, Missouri 63130, United States; orcid.org/0000-0001-6761-5868

Yang Lu — Institute of Materials Science & Engineering, Washington University, St. Louis, Missouri 63130, United States; Present Address: School of Engineering and Applied Sciences, Harvard University, Boston, MA 02134.

Hongmin Wang — Department of Chemistry, Washington University, St. Louis, Missouri 63130, United States; Present Address: Department of Chemistry, Yale University, New Haven, CT 06520.; orcid.org/0000-0003-2714-4250

Reagan Woon – Department of Chemistry, Washington University, St. Louis, Missouri 63130, United States; Present Address: Springer Nature, London N1 9XW, U.K.

Alina Chow — Department of Chemistry, Washington University, St. Louis, Missouri 63130, United States; Present Address: Department of Chemistry, Rice University, Houston, TX 77005.

Chiemela Izima — Department of Chemistry, Washington University, St. Louis, Missouri 63130, United States; Present Address: Vagelos College of Physicians and Surgeons, Columbia University, NY 10032.

Brandon Chow — Department of Chemistry, Washington University, St. Louis, Missouri 63130, United States; Present Address: University of Illinois College of Medicine, Chicago, IL 60612.

Complete contact information is available at: https://pubs.acs.org/10.1021/accountsmr.3c00031

#### **Author Contributions**

The manuscript was written through contributions of all authors. All authors have given approval to the final version of the manuscript.

#### **Author Contributions**

These authors contributed equally: Yifan Diao and Haoru Yang.

#### **Notes**

The authors declare no competing financial interest.

#### **Biographies**

Yifan Diao received his Ph.D. in 2021 from the Institute of Material Science and Engineering at Washington University in St. Louis under the supervision of Prof. Julio M. D'Arcy. He received his M.S. and B.S. from Washington University in St. Louis and Southwest Jiaotong University in 2017 and 2015, respectively. His doctoral research focuses on vapor-phase polymerization, iron hydrolysis, conducting polymer, nanofabrication, energy storage, flexible electronics, solar cells, CO<sub>2</sub> reduction, and antimicrobials.

Haoru Yang received his Ph.D. in 2023 from the Chemistry Department at Washington University in St. Louis under the supervision of Prof. Julio M. D'Arcy. He received his B.A. in 2018 from Washington University in St. Louis. His research focuses on vapor-phase synthesis and processing of nanostructured conducting polymers, electrochemical characterizations of conducting polymers, and 3D printing.

Yang Lu received his Ph.D. in 2021 from the Institute of Materials Science and Engineering at Washington University in St. Louis under the supervision of Prof. Julio M. D'Arcy. He received an M.S. degree in the Department of Electrical and Systems Engineering from Washington University in St. Louis in 2016 and received a B.S. degree from Huazhong University of Science and Technology in 2013. His

doctoral research focuses on vapor-phase polymerization, aerosol flow synthesis, conducting polymer characterizations, 3D printing, colloidal processing, and photothermal and electrochemical catalysis.

Hongmin Wang received his Ph.D. in 2021 from the Chemistry Department at Washington University in St. Louis under the supervision of Prof. Julio M. D'Arcy. He received an honored B.S. degree from College of Chemistry and Molecular Sciences, Wuhan University in 2016. His doctoral research focuses on vapor-phase polymerization, conducting polymers, inorganic—organic hybrid nanomaterials, and energy storage.

Reagan Woon received her B.A. in 2021 from Washington University in St. Louis and worked as an undergraduate researcher under the supervision of Prof. Julio M. D'Arcy.

Alina Chow received her B.A. in 2020 from Washington University in St. Louis and worked as an undergraduate researcher under the supervision of Prof. Julio M. D'Arcy.

**Chiemela Izima** received his B.A. in 2021 from Washington University in St. Louis and worked as an undergraduate researcher under the supervision of Prof. Julio M. D'Arcy.

**Brandon Chow** received his B.A. in 2022 from Washington University in St. Louis and worked as an undergraduate researcher under the mentorship of Prof. Julio M. D'Arcy.

Julio M. D'Arcy is an Assistant Professor of Chemistry and Carl J. and Anna Carlson Endowed Chair at Clark University. He is also an Honorary Professor of Chemistry at Washington University in St. Louis. His group aims to develop vapor-phase synthetic strategies that target novel organic nanostructured materials such as low dimensional conducting polymers for energy storage applications. Research in his laboratory seeks to advance the understanding of vapor-phase growth mechanisms and control deposition of crystalline hierarchical architectures that enhance rates of intra- and interchain energy transfer. His group applies these materials and fabricates electrochemical capacitors via robust engineering strategies that maximize material utilization yield at the electrode/electrolyte interface. He earned a B.A. from the State University of New York at Purchase and a Ph.D. in Chemistry from UCLA (2012) under the supervision of Prof. Richard Kaner and carried out his postdoctoral studies at MIT in the laboratory of Prof. Paula Hammond.

#### ACKNOWLEDGMENTS

The authors gratefully acknowledge funding from National Science Foundation (NSF CAREER 2144977). The authors also thank Dr. Huafang Li from the Institute of Material Science and Engineering at Washington University in St. Louis for her help with electron microscopy, Mr. James Linders and Mr. James Graflage from the machine shop in Chemistry Department at Washington University in St. Louis for their help in designing and building vapor-phase reactors, and Prof. Anne Hofmeister from Earth and Planetary Sciences Department at Washington University in St. Louis for sharing her expertise.

#### REFERENCES

- (1) Morris, R. V.; Golden, D. C.; Bell, J. F., III Low-Temperature Reflectivity Spectra of Red Hematite and the Color of Mars. *J. Geophys. Res. Planets* **1997**, *102* (E4), 9125–9133.
- (2) Mikucki, J. A.; Pearson, A.; Johnston, D. T.; Turchyn, A. V.; Farquhar, J.; Schrag, D. P.; Anbar, A. D.; Priscu, J. C.; Lee, P. A. A Contemporary Microbially Maintained Subglacial Ferrous "Ocean. *Science* **2009**, 324 (5925), 397–400.

- (3) Bora, D. K.; Braun, A.; Constable, E. C. in Rust We Trust". Hematite-the Prospective Inorganic Backbone for Artificial Photosynthesis. *Energy Environ. Sci.* **2013**, 6 (2), 407–425.
- (4) Salunkhe, T. T.; Varma, R. S.; Kadam, A. N.; Lee, S.-W.; Lee, Y.-C.; Hur, J.; Kim, I. T. Scraps to Superior Anodes for Li-Ion Batteries: Sustainable and Scalable Upgrading of Waste Rust. *J. Hazard. Mater.* **2021**, *410*, No. 124571.
- (5) Gurav, R.; Surve, S. K.; Babar, S.; Choudhari, P.; Patil, D.; More, V.; Sankpal, S.; Hangirgekar, S. Rust-Derived Fe2O3 Nanoparticles as a Green Catalyst for the One-Pot Synthesis of Hydrazinyl Thiazole Derivatives. *Org. Biomol. Chem.* **2020**, *18* (24), 4575–4582.
- (6) Babar, S.; Gavade, N.; Shinde, H.; Mahajan, P.; Lee, K. H.; Mane, N.; Deshmukh, A.; Garadkar, K.; Bhuse, V. Evolution of Waste Iron Rust into Magnetically Separable G-C3N4-Fe2O3 Photocatalyst: An Efficient and Economical Waste Management Approach. ACS Appl. Nano Mater. 2018, 1 (9), 4682-4694.
- (7) Diao, Y.; Chen, H.; Lu, Y.; Santino, L. M.; Wang, H.; D'Arcy, J. M. Converting Rust to PEDOT Nanofibers for Supercapacitors. *ACS Appl. Energy Mater.* **2019**, 2 (5), 3435–3444.
- (8) Lawal, A. T.; Wallace, G. G. Vapour Phase Polymerisation of Conducting and Non-Conducting Polymers: A Review. *Talanta* **2014**, *119*, 133–143.
- (9) Malinauskas, A. Chemical Deposition of Conducting Polymers. *Polymer (Guildf)* **2001**, 42 (9), 3957–3972.
- (10) Wang, H.; Diao, Y.; Rubin, M.; Santino, L. M.; Lu, Y.; D'Arcy, J. M. Metal Oxide-Assisted PEDOT Nanostructures via Hydrolysis-Assisted Vapor-Phase Polymerization for Energy Storage. *ACS Appl. Nano Mater.* **2018**, *1* (3), 1219–1227.
- (11) Jolivet, J.-P.; Chanéac, C.; Tronc, E. Iron Oxide Chemistry. From Molecular Clusters to Extended Solid Networks. *Chem. Commun.* **2004**, *5*, 481–483.
- (12) Li, D.; Huang, J.; Kaner, R. B. Polyaniline Nanofibers: A Unique Polymer Nanostructure for Versatile Applications. *Acc. Chem. Res.* **2009**, 42 (1), 135–145.
- (13) Flynn, C. M. Hydrolysis of Inorganic Iron(III) Salts. *Chem. Rev.* **1984**, *84* (1), 31–41.
- (14) Ebrahim, S.; Shokry, A.; Ibrahim, H.; Soliman, M. Polyaniline/Akaganéite Nanocomposite for Detoxification of Noxious Cr(VI) from Aquatic Environment. *Journal of Polymer Research* **2016**, 23 (4), 79.
- (15) Wei, G.; Du, K.; Zhao, X.; Li, C.; Li, J.; Ren, K.; Huang, Y.; Wang, H.; Yao, S.; An, C. Integrated FeOOH Nanospindles with Conductive Polymer Layer for High-Performance Supercapacitors. *J. Alloys Compd.* **2017**, 728, 631–639.
- (16) Wang, L.; Yang, H.; Liu, X.; Zeng, R.; Li, M.; Huang, Y.; Hu, X. Constructing Hierarchical Tectorum-like α-Fe2O3/PPy Nanoarrays on Carbon Cloth for Solid-State Asymmetric Supercapacitors. *Angew. Chem.* **2017**, *129* (4), 1125–1130.
- (17) Fahlman, M.; Fabiano, S.; Gueskine, V.; Simon, D.; Berggren, M.; Crispin, X. Interfaces in Organic Electronics. *Nat. Rev. Mater.* **2019**, *4* (10), 627–650.
- (18) Xue, Y.; Chen, S.; Yu, J.; Bunes, B. R.; Xue, Z.; Xu, J.; Lu, B.; Zang, L. Nanostructured Conducting Polymers and Their Composites: Synthesis Methodologies, Morphologies and Applications. *J. Mater. Chem. C Mater.* **2020**, *8* (30), 10136–10159.
- (19) Lu, Y.; Kacica, C.; Bansal, S.; Santino, L. M.; Acharya, S.; Hu, J.; Izima, C.; Chrulski, K.; Diao, Y.; Wang, H.; Yang, H.; Biswas, P.; Schaefer, J.; D'Arcy, J. M. Synthesis of Submicron PEDOT Particles of High Electrical Conductivity via Continuous Aerosol Vapor Polymerization. ACS Appl. Mater. Interfaces 2019, 11 (50), 47320–47329.
- (20) Santino, L. M.; Hwang, E.; Diao, Y.; Lu, Y.; Wang, H.; Jiang, Q.; Singamaneni, S.; D'Arcy, J. M. Condensing Vapor Phase Polymerization (CVPP) of Electrochemically Capacitive and Stable Polypyrrole Microtubes. ACS Appl. Mater. Interfaces 2017, 9 (47), 41496–41504.
- (21) Cho, B.; Park, K. S.; Baek, J.; Oh, H. S.; Koo Lee, Y.-E.; Sung, M. M. Single-Crystal Poly(3,4-Ethylenedioxythiophene) Nanowires with Ultrahigh Conductivity. *Nano Lett.* **2014**, *14* (6), 3321–3327.

- (22) Im, S. G.; Gleason, K. K. Systematic Control of the Electrical Conductivity of Poly(3,4-Ethylenedioxythiophene) via Oxidative Chemical Vapor Deposition. *Macromolecules* **2007**, 40 (18), 6552–6556
- (23) D'Arcy, J. M.; El-Kady, M. F.; Khine, P. P.; Zhang, L.; Lee, S. H.; Davis, N. R.; Liu, D. S.; Yeung, M. T.; Kim, S. Y.; Turner, C. L.; Lech, A. T.; Hammond, P. T.; Kaner, R. B. Vapor-Phase Polymerization of Nanofibrillar Poly(3,4- Ethylenedioxythiophene) for Supercapacitors. *ACS Nano* **2014**, 8 (2), 1500–1510.
- (24) Yoon, H.; Chang, M.; Jang, J. Formation of 1D Poly(3,4-Ethylenedioxythiophene) Nanomaterials in Reverse Microemulsions and Their Application to Chemical Sensors. *Adv. Funct. Mater.* **2007**, 17 (3), 431–436.
- (25) He, W.; Wang, C.; Zhuge, F.; Deng, X.; Xu, X.; Zhai, T. Flexible and High Energy Density Asymmetrical Supercapacitors Based on Core/Shell Conducting Polymer Nanowires/Manganese Dioxide Nanoflakes. *Nano Energy* **2017**, *35*, 242–250.
- (26) Wang, J.; Zhu, C.; Han, J.; Han, N.; Xi, J.; Fan, L.; Guo, R. Controllable Synthesis of Gold Nanorod/Conducting Polymer Core/Shell Hybrids Toward in Vitro and in Vivo near-Infrared Photothermal Therapy. ACS Appl. Mater. Interfaces 2018, 10 (15), 12323—12330.
- (27) Wang, Y.; Zhang, W.; Wu, X.; Luo, C.; Wang, Q.; Li, J.; Hu, L. Conducting Polymer Coated Metal-Organic Framework Nanoparticles: Facile Synthesis and Enhanced Electromagnetic Absorption Properties. *Synth. Met.* **2017**, 228, 18–24.
- (28) Jun, J.; Lee, J. S.; Shin, D. H.; Oh, J.; Kim, W.; Na, W.; Jang, J. Fabrication of a One-Dimensional Tube-in-Tube Polypyrrole/Tin Oxide Structure for Highly Sensitive DMMP Sensor Applications. *J. Mater. Chem. A Mater.* **2017**, *5* (33), 17335–17340.
- (29) Musić, S.; Maljković, M.; Czakó-Nagy, I. Effect of Urea on the Hydrolysis of Fe3+ Ions in Aqueous Solutions at Elevated Temperature. *Mater. Lett.* **1997**, *31* (1), 43–48.
- (30) Arab, F.; Mousavi-Kamazani, M.; Salavati-Niasari, M. Synthesis, Characterization, and Optical Properties of Te, Te/TeO2 and TeO2 Nanostructures via a One-Pot Hydrothermal Method. *RSC Adv.* **2016**, 6 (75), 71472–71480.
- (31) Wang, H.; Rogach, A. L. Hierarchical SnO2 Nanostructures: Recent Advances in Design, Synthesis, and Applications. *Chem. Mater.* **2014**, *26* (1), 123–133.
- (32) Martín, S. E.; Suárez, D. F. Catalytic Aerobic Oxidation of Alcohols by Fe(NO3)3–FeBr3. *Tetrahedron Lett.* **2002**, 43 (25), 4475–4479.
- (33) Wang, H.; Santino, L. M.; Rubin, M.; Diao, Y.; Lu, Y.; D'Arcy, J. M. Self-Woven Nanofibrillar PEDOT Mats for Impact-Resistant Supercapacitors. *Sustain. Energy Fuels* **2019**, *3* (5), 1154–1162.
- (34) Snook, G. A.; Kao, P.; Best, A. S. Conducting-Polymer-Based Supercapacitor Devices and Electrodes. *J. Power Sources* **2011**, *196* (1), 1–12.
- (35) Naskar, P.; Maiti, A.; Chakraborty, P.; Kundu, D.; Biswas, B.; Banerjee, A. Chemical Supercapacitors: A Review Focusing on Metallic Compounds and Conducting Polymers. *J. Mater. Chem. A Mater.* **2021**, 9 (4), 1970–2017.
- (36) Dunn, B.; Kamath, H.; Tarascon, J.-M. Electrical Energy Storage for the Grid: A Battery of Choices. *Science* **2011**, 334 (6058), 928–935.
- (37) Wang, Y.-X.; Zhang, B.; Lai, W.; Xu, Y.; Chou, S.-L.; Liu, H.-K.; Dou, S.-X. Room-Temperature Sodium-Sulfur Batteries: A Comprehensive Review on Research Progress and Cell Chemistry. *Adv. Energy Mater.* **2017**, *7* (24), 1602829.
- (38) Wang, H.; Diao, Y.; Lu, Y.; Yang, H.; Zhou, Q.; Chrulski, K.; D'Arcy, J. M. Energy Storing Bricks for Stationary PEDOT Supercapacitors. *Nat. Commun.* **2020**, *11* (1), 3882.
- (39) Kreimeyer, R. Some Notes on the Firing Colour of Clay Bricks. *Appl. Clay Sci.* **1987**, 2 (2), 175–183.
- (40) Kyeremateng, N. A.; Brousse, T.; Pech, D. Microsupercapacitors as Miniaturized Energy-Storage Components for on-Chip Electronics. *Nat. Nanotechnol.* **2017**, *12* (1), 7–15.

- (41) Pech, D.; Brunet, M.; Taberna, P.-L.; Simon, P.; Fabre, N.; Mesnilgrente, F.; Conédéra, V.; Durou, H. Elaboration of a Microstructured Inkjet-Printed Carbon Electrochemical Capacitor. *J. Power Sources* **2010**, *195* (4), 1266–1269.
- (42) El-Kady, M. F.; Strong, V.; Dubin, S.; Kaner, R. B. Laser Scribing of High-Performance and Flexible Graphene-Based Electrochemical Capacitors. *Science* **2012**, 335 (6074), 1326–1330.
- (43) Lang, X.; Hirata, A.; Fujita, T.; Chen, M. Nanoporous Metal/Oxide Hybrid Electrodes for Electrochemical Supercapacitors. *Nat. Nanotechnol.* **2011**, *6* (4), 232–236.
- (44) Zhang, C. J.; Kremer, M. P.; Seral-Ascaso, A.; Park, S.-H.; McEvoy, N.; Anasori, B.; Gogotsi, Y.; Nicolosi, V. Microelectronics: Stamping of Flexible, Coplanar Micro-Supercapacitors Using MXene Inks (Adv. Funct. Mater. 9/2018). *Adv. Funct. Mater.* **2018**, 28 (9), No. 1870059.
- (45) Diao, Y.; Lu, Y.; Yang, H.; Wang, H.; Chen, H.; D'Arcy, J. M. Direct Conversion of Fe2O3 to 3D Nanofibrillar PEDOT Microsupercapacitors. *Adv. Funct. Mater.* **2020**, *30* (32), No. 2003394.
- (46) Grätzel, M. Recent Advances in Sensitized Mesoscopic Solar Cells. Acc. Chem. Res. 2009, 42 (11), 1788–1798.
- (47) Briscoe, J.; Dunn, S. Dye-Sensitized Solar Cells: The Future of Using Earth-Abundant Elements in Counter Electrodes for Dye-Sensitized Solar Cells (Adv. Mater. 20/2016). *Adv. Mater.* **2016**, 28 (20), 3976.
- (48) Kouhnavard, M.; Ludin, N. A.; Ghaffari, B. V.; Sopian, K.; Ikeda, S. Carbonaceous Materials and Their Advances as a Counter Electrode in Dye-Sensitized Solar Cells: Challenges and Prospects. *ChemSusChem* **2015**, *8* (9), 1510–1533.
- (49) Kouhnavard, M.; Yifan, D.; D'Arcy, J. M.; Mishra, R.; Biswas, P. Highly Conductive PEDOT Films with Enhanced Catalytic Activity for Dye-Sensitized Solar Cells. *Sol. Energy* **2020**, *211*, 258–264.
- (50) Prigodin, V. N.; Epstein, A. J. Nature of Insulator–Metal Transition and Novel Mechanism of Charge Transport in the Metallic State of Highly Doped Electronic Polymers. *Synth. Met.* **2001**, *125* (1), 43–53.
- (51) Cheng, M.; Yang, X.; Chen, C.; Zhao, J.; Zhang, F.; Sun, L. Dye-Sensitized Solar Cells Based on Hydroquinone/Benzoquinone as Bio-Inspired Redox Couple with Different Counter Electrodes. *Phys. Chem. Chem. Phys.* **2013**, *15* (36), 15146–15152.
- (52) Li, Y.; Shimada, H.; Sakairi, M.; Shigyo, K.; Takahashi, H.; Seo, M. Formation and Breakdown of Anodic Oxide Films on Aluminum in Boric Acid/Borate Solutions. *J. Electrochem. Soc.* **1997**, *144* (3), 866–876.
- (53) Huang, Z.; Hao, Y.; Li, Y.; Hu, H.; Wang, C.; Nomoto, A.; Pan, T.; Gu, Y.; Chen, Y.; Zhang, T.; Li, W.; Lei, Y.; Kim, N.; Wang, C.; Zhang, L.; Ward, J. W.; Maralani, A.; Li, X.; Durstock, M. F.; Pisano, A.; Lin, Y.; Xu, S. Three-Dimensional Integrated Stretchable Electronics. *Nat. Electron.* **2018**, *1* (8), 473–480.
- (54) Tang, Y.; Li, Y.; Hong, Y.; Yang, S.; Yin, J. Programmable Active Kirigami Metasheets with More Freedom of Actuation. *Proc. Natl. Acad. Sci. U. S. A.* **2019**, *116* (52), 26407–26413.
- (55) Diao, Y.; Woon, R.; Yang, H.; Chow, A.; Wang, H.; Lu, Y.; D'Arcy, J. M. Kirigami Electrodes of Conducting Polymer Nanofibers for Wearable Humidity Dosimeters and Stretchable Supercapacitors. *J. Mater. Chem. A Mater.* **2021**, *9* (15), 9849–9857.
- (56) Leung, N. H. L.; Chu, D. K. W.; Shiu, E. Y. C.; Chan, K.-H.; McDevitt, J. J.; Hau, B. J. P.; Yen, H.-L.; Li, Y.; Ip, D. K. M.; Peiris, J. S. M.; Seto, W.-H.; Leung, G. M.; Milton, D. K.; Cowling, B. J. Respiratory Virus Shedding in Exhaled Breath and Efficacy of Face Masks. *Nat. Med.* **2020**, *26* (5), *676*–*680*.
- (57) Huang, L.; Xu, S.; Wang, Z.; Xue, K.; Su, J.; Song, Y.; Chen, S.; Zhu, C.; Tang, B. Z.; Ye, R. Self-Reporting and Photothermally Enhanced Rapid Bacterial Killing on a Laser-Induced Graphene Mask. ACS Nano 2020, 14 (9), 12045—12053.
- (58) Françon, H.; Wang, Z.; Marais, A.; Mystek, K.; Piper, A.; Granberg, H.; Malti, A.; Gatenholm, P.; Larsson, P. A.; Wågberg, L. Ambient-Dried, 3D-Printable and Electrically Conducting Cellulose Nanofiber Aerogels by Inclusion of Functional Polymers. *Adv. Funct. Mater.* **2020**, *30* (12), 1909383.

- (59) Panapoy, M.; Singsang, W.; Ksapabutr, B. Electrically Conductive Poly(3,4-Ethylenedioxythiophene)—Poly(Styrene Sulfonate)/Polyacrylonitrile Fabrics for Humidity Sensors. *Phys. Scr.* **2010**, *T139*, 14056.
- (60) Huang, J.; Virji, S.; Weiller, B. H.; Kaner, R. B. Polyaniline Nanofibers: Facile Synthesis and Chemical Sensors. *J. Am. Chem. Soc.* **2003**, *125* (2), 314–315.

#### **□** Recommended by ACS

### Iron-Gold Composites for Biodegradable Implants: *In Vitro* Investigation on Biodegradation and Biomineralization

V. P. Muhammad Rabeeh, T. Hanas, et al.

JUNE 15, 2023

ACS BIOMATERIALS SCIENCE & ENGINEERING

READ 🗹

#### Continuous-Flow Chemical Synthesis for Sub-2 nm Ultra-Multielement Alloy Nanoparticles Consisting of Group IV to XV Elements

Hiroki Minamihara, Hiroshi Kitagawa, et al.

JULY 20, 2023

JOURNAL OF THE AMERICAN CHEMICAL SOCIETY

READ 🗹

### Gradience Free Nanoinsertion of Fe<sub>3</sub>O<sub>4</sub> into Wood for Enhanced Hydrovoltaic Energy Harvesting

Ying Gao, Yuanyuan Li, et al.

JULY 13, 2023

ACS SUSTAINABLE CHEMISTRY & ENGINEERING

READ [7

#### Fluid-Assisted Aggregation and Assembly of Magnetite Microparticles in the Giant El Laco Iron Oxide Deposit, Central Andes

J. Tomás Ovalle, Diego Morata, et al.

MAY 15, 2023

ACS EARTH AND SPACE CHEMISTRY

READ 🗹

Get More Suggestions >